Enhanced Cu-Ni-TiO_2-BP Plasmonic Biosensor for Highly Sensitive Biomolecule Detection and SARS-CoV-2 Diagnosis

Shivam Singh, Anurag Upadhyay, Bhargavi Chaudhary, *Student Member, IEEE,* Kapil Sirohi and Santosh Kumar, *Senior Member, IEEE*

***Abstract*— In this work, a bimetallic (Cu-Ni) prism-based surface plasmon resonance (SPR) sensor is presented. To enhance the interaction of bio-analytes with sensing surface, a 2-D nanomaterial black phosphorous (BP) is used as it exhibits high biomolecule adsorption on its surface. Our investigation includes an assessment of key performance parameters such as sensitivity (S), full width at half maximum (FWHM), detection accuracy (DA), figure of merit (FoM), and penetration depth (PD). We meticulously optimized the thicknesses of the Copper, Nickel, and TiO_2 layers to achieve optimal sensor performance. Our findings demonstrate that the highest sensitivity (S) is achieved with a configuration comprising a 25 nm layer of Cu, a 20 nm layer of Ni, a 1 nm layer of TiO_2, and a monolayer of BP, resulting in a remarkable sensitivity (S) of 516°/RIU, with remarkable DA, FWHM and FoM of 0.20/°, 6.15° and 83.59/RIU, respectively. The incorporation of the TiO_2 layer between the Ni and BP layers contributes to the enhanced sensitivity. Additionally, our proposed sensor configuration is well-suited for the detection of biomolecules within the refractive index (RI) range of 1.330-1.335. We further assessed the sensor's capabilities in detecting the SARS-CoV-2 coronavirus, which exhibits RI values falling within the considered range (1.3348 and 1.3398). After optimizing the thickness of the metal layers, our sensor achieves an optimal sensitivity of 502°/RIU for SARS-CoV-2 virus detection. This configuration also maintains excellent DA, FWHM, and FoM values of 0.20/°, 4.9°, and 100.56/RIU, respectively.**

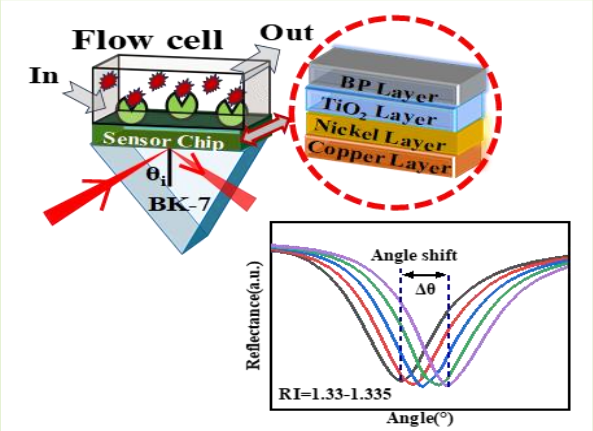

***Index Terms*— Surface Plasmon Resonance (SPR), Plasmonic Biosensor, Black Phosphorous (BP), Cu-Ni-TiO_2 Hybrid Structure SARS-CoV-2 Detection**

I. Introduction

OPTICAL SPR biosensors have garnered considerable interest among scientists and researchers owing to their substantial advantages over conventional biosensors such as higher sensitivity, label-free detection capabilities, cost-effectiveness, and real-time monitoring capabilities [1]. Optical sensors find extensive utility across a spectrum of sensing applications, including but not limited to chemical sensing, biosensing, glucose monitoring, and medical diagnostics [2]-[5]. The elementary principle of SPR sensor is to analyze the change in input light and corresponding parametric variations in the output light e.g., phase, amplitude, angle or polarization of light [6]. The SPR sensors are very sensitive to the change in refractive index (RI) of the analyte [7]. In order to have the SPR phenomenon, the input light must be p-polarized, and the phase of the input light should be

The work of Santosh Kumar was supported in part by the Double-Hundred Talent Plan of Shandong Province, China: in part by the Liaocheng University under Grant 318052341 and in part by the Science and Technology Support Plan for Youth Innovation of Colleges and Universities of Shandong Province of China under Grant 2022KJ107. (Corresponding authors: Bhargavi Chaudhary: Santosh Kuimar.)

Shivam Singh is with Department of ECE, ABES Engineering College Ghaziabad, Uttar Pradesh 201009, India(e-mail:shivams20@gmail.com)

Anurag Upadhyay is with Department of ASH, Rajkiya Engineering College Azamgarh,Uttar Pradesh 276201, India (e-mail:anurag.upadhyay009@gmail.com)

Bhargavi Chaudhary is with Department of EE, Indian Institute of Technology Delhi, New Delhi 110016, India(e-mail-bhargavichy31@yahoo.com)

Kapil Sirohi is with Department of ECE, University Institute of Engineering and Technology (UIET), M.D. University Rohtak, Haryana 124001, India(e-mail:kpsirohi2@gmail.com)

Santosh Kumar is with the Shandong Key Laboratory of Optical Communication Science and Technology, School of Physics Science and Information Technology, Liaocheng University, Liaocheng 252059, China, and also with the Department of Electronics and Communication Engineering, K. L. Deemed to be University, Guntur, Andhra Pradesh 522302, India (e-mail: santosh@lcu.edu.cn).

matched with the surface plasmon (SP) wave vector (resonance condition) generated at prism-metal interface [8]. The SPR sensor identifies the biomolecules on its surface when input light is illuminated at the interface. A sharp dip for a particular RI resulted in the resonance condition that occurred in the SPR sensor, which is termed the reflective intensity curve. Changing the analyte RI leads to a shift in the position and a dip in the reflectivity curve, occurring at different angles. Consequently, due to their simple operation and remarkable sensitivity, SPR sensors surpass contemporary optical techniques like planar waveguides, Bragg gratings, and Raman scattering in terms of versatility and applicability [9], [10]. Otto and Kretschmann configurations are two viable setups for SPR-based sensors. However, the Kretschmann configuration, especially when combined with angular interrogation, has demonstrated superior performance due to its lower power consumption [11]. Typically, this setup employs a low-RI prism, such as BK-7 or SF-10, as its base. The prism base is coated a the metal layer such as gold (Au), silver (Ag), copper (Cu), and nickel (Ni) due to their superb optical properties [12]-[14]. Silver exhibits a sharper SPR curve, but it is susceptible to oxidation, restricting its long-term durability. Further, Au has limited molecular adsorption, resulting in poor sensitivity. Cu exhibits good behaviour, but generates fewer SPs than Ag and Au. However, it offers greater long-term reliability due to lower susceptibility to oxidation. To enhance performance and oxidation resistance, researchers have explored bimetallic SPR sensors by combining two metals with complementary plasmonic properties, making them suitable for a range of sensing applications [15]. Srivastava et al., in their literature, showed the different bimetal SPR sensors with two different metals such as Au-Cu, Au-Ag, and Au-Al [24]. TiO_2 can be used to prevent the oxidation of metals as well as enhance their sensitivity [3]. In recent years, two-dimensional (2-D) nanomaterials have displayed the potential to significantly enhance sensor performance due to their exceptional optical and electronic properties [16]-[18]. Numerous 2-D materials have been applied in SPR sensing due to their favorable adsorption energies and physiochemical properties for binding molecules [19],[20]. Among these, graphene has been the primary 2-D nanomaterial of choice in sensing applications [21]. Additionally, black phosphorous (BP) is a commonly used 2-D material in optoelectronic sensing due to its graphene-like structure and the ability to be exfoliated into ultrathin nanosheets [22]. Nangare et al. reported that BP can speed up the sensitivity response up to 40 times faster than other 2-D nanomaterials [23]. In 2021, Singh et al. delineated the SPR sensor using BP for chemical sensing and obtained sensitivity as 218 (°/RIU) [24]. In 2022, Vasimalla et al. theoretically investigated the SPR structure with BP layer for hemoglobin and glucose detection in blood and urine respectively [25].

Nowadays, SPR biosensors are frequently used in disease detection due to their instantaneous and real time responses. In this connection, an outbreak of a human conveyable virus named SARS-CoV-2 caused millions of deaths worldwide [26]. This virus attacks the human respiratory system and easily transfers through the air. Hence, its eruption was proclaimed a global pandemic by the WHO. SARS-CoV-2 is composed of positive single wattled RNA and four structural proteins (S, E, M, and N). It enters human cells by binding to angiotensin-converting enzyme 2 (ACE2), which is a membrane protein (spike glycoprotein S) [27]. The vital organs of the human body, such as the lungs, kidneys, heart, and brain, face serious injury from the activation of S-protein [28]. Hence, in order to stop the proliferation of viruses, it has become mandatory to counteract the activation of the S-protein. Many vaccines are presently available and effective against SARS-CoV-2 to save lives. However, the mutation ability leads to a rapid outbreak of viruses [29]. Therefore, it is mandatory to detect the virus at an early stage to curb the pandemic. The primary method for detecting the virus is reverse transcriptase polymerase chain reaction (RT-PCR), which takes 1-3 days to yield results [30]. RT-PCR has an approximate sensitivity of 60%. Another testing method is a rapid antigen test available for SARS-CoV-2. However, these reported methods of detection are sluggish. Therefore, optical biosensors, especially SPR-based ones, offer a fast and precise alternative for SARS-CoV-2 detection [31]. In our work, we have directed our efforts towards the exploration of a SPR sensor, aimed at enhancing its performance parameters for potential application in the detection of SARS-CoV-2. As shown in Fig.1, the proposed SPR sensor configuration comprises a BK-7 prism, a bimetallic layer composed of Cu and Ni, a layer of TiO_2, and a BP layer, all arranged in sequence with the sensing medium (SM). To assess and visualize the performance characteristics of this setup, we generated performance parameter plots and electric field distributions using MATLAB and COMSOL Multiphysics. One notable aspect of our work is the inherent resistance to oxidation of the SPR chip, making it an economically viable alternative to conventional silver and gold based SPR sensors. It is important to highlight that there is limited prior research on the detection of SARS-CoV-2 using SPR technology. Notably, we have achieved an unprecedented level of sensitivity for SARS-CoV-2 detection, registering an impressive value of 502 (^{0}/RIU). This innovative approach holds promise for advancing the field of SPR-based biosensing, particularly in the context of virus detection.

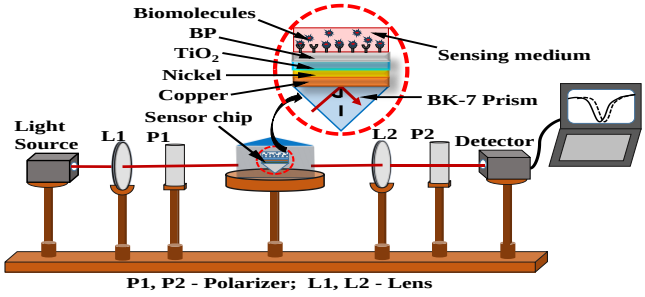

Fig. 1 Experimental arrangement of a proposed biosensor for detecting bio-analyte through angle interrogation.

II. Theoretical Modelling

In this section, we provide a thorough elucidation of the design parameters, software tools, and models that were employed in our simulations. We also present a detailed, step-by-step description of the simulation process carried out through the utilization of MATLAB and COMSOL Multiphysics software. Our simulation methodology relies on the Transfer Matrix Method (TMM) and the application of Fresnel equations within the MATLAB environment. Furthermore, to explore the distribution of fields at various layer interfaces in our proposed biosensor, we harnessed the Finite Element Method (FEM) capabilities offered by COMSOL Multiphysics.

A. Design synthesis

The proposed structure is designed in a Kretschmann configuration with prisms and coatings of different materials. The sensor is able to enhance the strength of the electric field at the sensing layer interface and can be utilized for long-range SPR in dip reflectance mode. We have investigated the effect of different thicknesses of bimetal layer (Cu-Ni), dielectric material (TiO_2), and 2-D material, i.e., BP, for the purpose of getting high sensitivity. In the proposed sensor, a BK-7 prism is used to launch the p-polarized monochromatic wave. Due to its low RI, it is easy to match the wave vector of a plasmonic wave with an incoming light wave, resulting in high surface plasmon polaritons (SPP's). The operating wavelength (λ_{op}) is chosen at 633 nm because it shows maximum SPP elevation in the range of 0.40 µm to 0.633 µm. The RI of the BK-7 prism can be evaluated using Eq.1 as follows [13]:

$$n_{pri}^2 = 1 + \frac{X_1\lambda_{op}^2}{\lambda_{op}^2 - Y_1} + \frac{X_2\lambda_{op}^2}{\lambda_{op}^2 - Y_2} + \frac{X_3\lambda_{op}^2}{\lambda_{op}^2 - Y_3} \quad (1)$$

where λ_{op} is operating wavelength in micrometers.

The Cu-Ni bilayer coating has been used over BK-7 prism whose RI can be calculated using Eq.2 based on the Drude model as given as:

$$n_{Cu/Ni}^2 = 1 - \frac{\lambda_C\lambda_{op}^2}{\lambda_p^2 * (\lambda_C + i * \lambda_{op})} \quad (2)$$

Here, the λ_p denotes the plasma wavelength and λ_C describes the collison wavelength of the metals and these values differ for Cu and Ni [21]. Additionally, the thickness and RIs of various constituent layers are shown in Table I.

TABLE I
THICKNESS AND RIS USED FOR VARIOUS LAYERS AT $\lambda = 633\,nm$

Layers used	Thickness (nm)	RI (n+ik)		Ref.
		Real (n)	Imaginary(k)	
Cu	20-60	0.0369	4.5393	[21]
Ni	5-20	0.0303	2.2843	
BP	0.53	3.53	0.0408	
TiO_2	1, 3, 5, 7	2.58	0.0	[3]

B. Mathematical Formulations

The structure is numerically analysed using TMM to get the optimized value of thickness of different layers for achieving a large dip and higher sensitivity. Moreover, the proposed structure is also simulated using the finite element method for calculating SPP mode and electric field strength at different interfaces of the suggested sensor structure. The results are very precise in TMM due to very few approximations used in this method. In our analysis, we are using a six layered structure stacked along the z-direction. SPR sensor property estimation along the z-axis is done in order to get the optimized thickness (t_z), permittivity (ε_z), refractive index (n_z) and permeability (μ_z). The tangential boundary conditions of the first boundary ($Z = Z_1 = 0$) and the last boundary ($Z = Z_{N-1}$) can be associated with the mathematical relation given as:

$$\begin{bmatrix} P_1 \\ Q_1 \end{bmatrix} = M \begin{bmatrix} P_{N-1} \\ Q_{N-1} \end{bmatrix} \quad (3)$$

where, P_1, Q_1, P_{N-1}, Q_{N-1} are the electric field and magnetic boundary conditions of the first and the last layer interfaces, respectively. The symbol M designates the characteristic equation for the proposed sensor that can be formulated as:

$$M = \prod_{t_z=2}^{t_z=N-1} M_{t_z} = \begin{bmatrix} m_{11} & m_{12} \\ m_{21} & m_{22} \end{bmatrix} \quad (4)$$

where, $M_{t_z} = \begin{bmatrix} cos\beta_{t_z} & -isin\beta_{t_z}/q_{t_z} \\ -iq_{t_z}sin\beta_{t_z} & cos\beta_{t_z} \end{bmatrix}$

$q_{t_z} = \frac{\sqrt{\varepsilon_{t_z} - n_1^2 sin^2\theta_{in}}}{\varepsilon_{t_z}}$, and $\beta_{t_z} = \frac{2\pi d_t}{\lambda_{op}}\sqrt{\varepsilon_{t_z} - n_1^2 sin^2\theta_{in}}$

Here, θ_{in} represents input angle, d_t denotes thickness of different layer and ε_{t_z} shows permittivity of different layers. The reflection coefficient (r) can be formulated as:

$$r = \frac{(m_{11} + m_{12}q_n)q_1 - (m_{21} + m_{22}q_n)}{(m_{11} + m_{12}q_n)q_1 - (m_{21} + m_{22}q_n)} \quad (5)$$

Therefore, the reflectance for the N layer proposed sensor can be calculated as: $R = |r|^2$

C. The Parametric Interpretation Estimastion

The performance parameters, as estimated below [25], [26], of the propounded sensor are thoroughly evaluated and found to be well convenient for sharp dip, high sensitivity, minimum FWHM (full width half maxima), large detection accuracy (DA), and high figure of merit (FoM) as compared to conventional SPR sensors. The most important performance parameter is sensitivity (S), which can be defined as the ratio of the change in resonance angle to the change in RI of the analyte in the sensing medium. The sensitivity is computed as:

$$S = \frac{d\theta_{reso}}{dn_a} (°/RIU) \quad (6)$$

The DA can be defined as the inverse ration of FWHM and can be expressed as:

$$DA = 1/FWHM\ (1/°) \quad (7)$$

Here, FWHM denotes the difference of points that are at 50% of the maximum value of the reflectance curve.

FoM is defined as the ratio of sensitivity against the FWHM of the reflectance curve and can be formulated as:

$$FoM = S/FWHM \quad (8)$$

III. RESULTS AND DISCUSSIONS

The proposed sensor achieved optimal results by optimizing thickness of its constituent layers for the refractive index (RI) range of sensing medium from 1.330 to 1.335, which covers various chemical and biological analytes.

A. *Effect of Metal Layers Thickness On Sensitivity and Their Optimization*

In order to interrogate the parametric performance of the sensor, we initially change the Ni layer thickness in step size for different values of TiO_2 layer thicknesses. Figs. 2(a)-(d) show the variations in sensitivity and reflectance minima versus change in Cu layer thickness (20 nm-60 nm) for different thickness values of the Ni layer in a step size of 5 nm with a fixed TiO_2 layer thickness. The observed maximum sensitivities are 316.61 (°/RIU), 339.64 (°/RIU), 377 (°/RIU), and 421.12 (°/RIU) for TiO_2 thickness of 1nm, 3 nm, 5 nm, 7 nm at Ni thickness 15 nm, as shown in Fig. 2(a)-(d). The performance parameters are optimized for maximum sensitivity and minimum reflectance both. From Fig. 2(a)-(d), it is clearly visible that R_{min} initially decreases and then increases after 40-43 nm, 45-50 nm, and 50-55 nm Cu layer thickness for Ni layer thickness 15 nm, 10 nm, 5 nm, respectively. Hence, the sensitivity increases with an increase in both the Cu layer thickness and the Ni layer thickness. The maximum sensitivity calculated is 421.12 (°/RIU) at the cost of R_{min} which equals to 9.18×10^{-5} (a.u.). Since, TiO_2 layer is used as an adhesive layer, its thickness should be minimum, as the highest FoM value achieved for 1 nm thickness. However, the maximum sensitivity is achieved for larger values of Ni thickness. Thus, in Fig. 2(e), we have taken a TiO_2 thickness of 1 nm and a Ni thickness of 20 nm in order to observe the performance parameter variation. The resulted maximum sensitivity and minimum reflectance values are 516 (°/RIU) and 1.39×10^{-2} (a.u.), respectively as seen from Fig. 2(e). Additionally, the performance parameters are adjusted in Table II for given structure at different values of metal bilayer thickness with fixed thickness of TiO_2 layer.

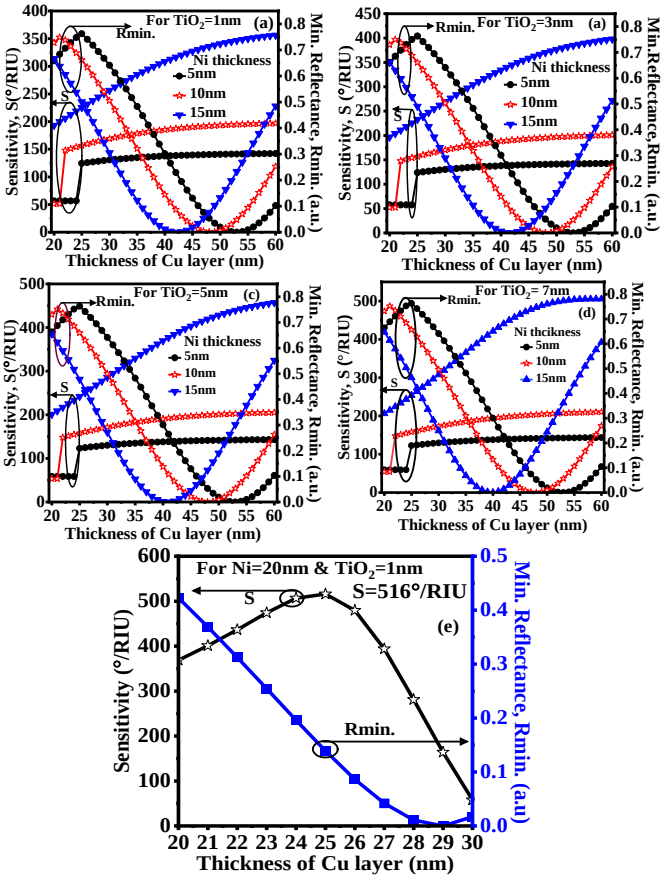

Fig. 2 Sensitivity and minimum reflectance vs. thickness of Cu layer for the structure BK7-Cu-Ni-TiO_2-BP-SM (a) Ni=5nm, 10nm, and 15nm for TiO_2=1 nm (b) Ni=5 nm, 10 nm, and 15 nm for TiO_2=3 nm (c) Ni=5 nm, 10 nm, and 15 nm for TiO_2=5 nm (d) (a) Ni=5 nm, 10 nm, and 15 nm for TiO_2=7 nm (e) Ni=20 nm for TiO_2=1 nm.

TABLE II
SENSITIVITY PERFORMANCE FOR DIFFERENT VALUES OF CU-NI LAYERS AT FIXED TIO_2 LAYER THICKNESS

Thickness (nm)			S	Rmin.	FWHM	DA	FoM
Cu	Ni	TiO_2	(°/RIU)	(a.u.)	(°)	(1/°)	(/RIU)
53	5	1	141.29	1.54×10^{-6}	0.85	1.18	166.72
48	10		192.28	2.47×10^{-4}	1.58	0.63	121.13
42	15		316.61	1.41×10^{-4}	3.1	0.32	101.31
53	5	3	141.74	4.82×10^{-6}	0.88	1.14	161.58
48	10		195.6	1.01×10^{-4}	1.66	0.6	117.36
41	15		339.64	9.74×10^{-4}	3.44	0.29	98.49
53	5	5	142.09	1.18×10^{-5}	0.92	1.08	153.45
48	10		199.5	1.25×10^{-5}	1.74	0.57	113.71
41	15		377	7.99×10^{-5}	3.71	0.27	101.79
53	5	7	142.43	2.35×10^{-5}	0.95	1.05	149.55
48	10		203.62	1.58×10^{-5}	1.82	0.55	111.99
40	15		421.12	9.18×10^{-5}	4.15	0.24	101.06
25	20	1	516	0.139	6.15	0.162	83.59

B. *Illustration of Refractive Index Sensing*

Figs. 3(a)-(d) display the curves plotted for reflectance intensity against the change in incident angle of TM-mode polarized input light to the proposed sensor structure for the sensing layer's RI values of 1.330 and 1.335 at different values of Ni and TiO_2 layer thickness. The solid curve represents the RI of 1.330, while the dashed curve shows RI of 1.335. From figures, it is clearly seen that largest sensitivity has been observed for Ni layer thickness equals to 15 nm and TiO_2 thickness sequals to 7 nm. But, the reflectance minima showed larger value with the aforesaid thickness values of Ni and TiO_2 which may create ambiguity at observation point. Thus, Fig. 3(e) is organized for TiO_2 layer thickness of 1 nm and Ni thickness of 20 nm.We perceived from SPR characteristics graph that largest change is observed for Cu-Ni bimetals with the use of BP monolayer using TiO_2 adhesion. The largest shift in resonance angle ($\Delta\theta$)

is obtained as, $\Delta\theta$=2.58°, as a result of RI variation of sensing layer from 1.33 to 1.335.

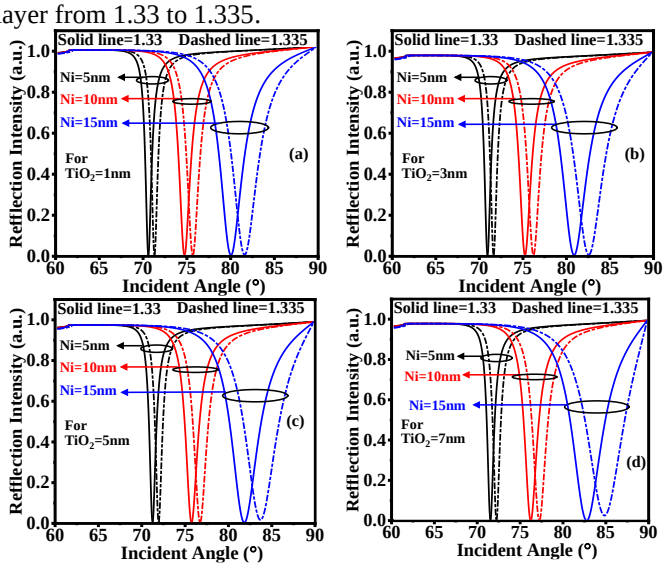

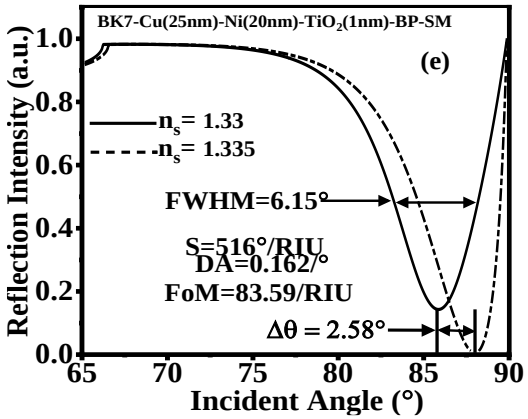

Fig.3 (a)-(e)The reflection Intensity vs Incident angle of various thickness of Cu, Ni, and TiO_2.

The Cu-Ni bimetal is used to enhance sensitivity because of their larger separation in work function values. The observed sensitivity is 516 (°/RIU) with FoM and detection accuracy (DA) values are 83.59 (/RIU) and 0.162 (/°).

Apart from sensitivity, the other major performance parameters have also been investigated at the optimized thickness of Cu, Ni, and TiO_2 and BP layers, as shown in Fig. 4. Fig. 4(a) displays SPR characteristic curves, which are plotted between reflectance intensity and resonant angle for RI variation from 1.330 to 1.335 at thicknesses of 25 nm, 20 nm, and 1 nm, respectively. Additionally, Figs. 4(b) and 4(c) show the graph of sensitivity, reflectance minima DA, and FoM against the RI variation of the sensing medium. It is seen from Fig. 4(b) that sensitivity initially increases, and then after RI value 1.334, it is decreasing. On the contrary, the Rmin decreases with RI values. Hence, the maximum sensitivity and the corresponding Rmin values are 516 (°/RIU) and 1.39×10^{-2} (a.u.). Whereas, from Fig. 4(c), it is observed that DA increases after RI 1.332 and FoM increases with an increase in RI values. Therefore, the maximum observed values of DA and FoM are 0.167 (/°) and 86.21 (/RIU), respectively

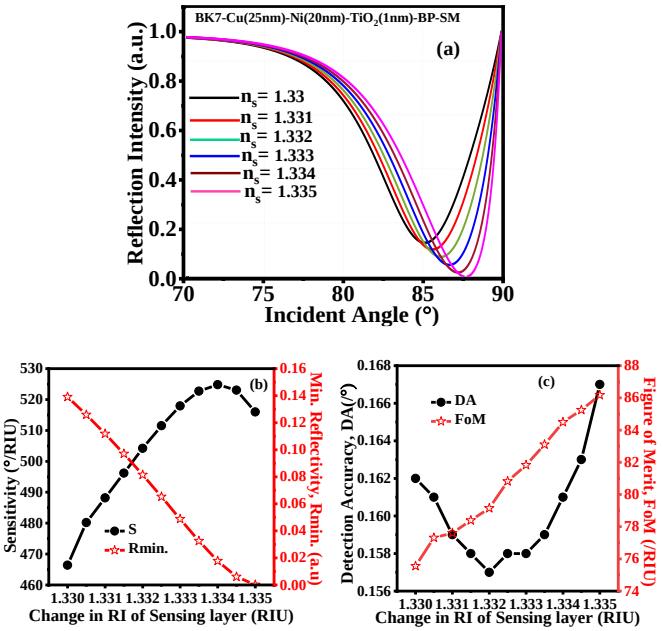

Fig. 4(a) Reflectance curve vs Incident angle at various RI of sensing layer (b) Sensitivity, Rmin (c) DA, FoM vs Change in RI of sensing layer respectively of proposed SPR sensor.

C. *Assessment of Electromagnetic Field Utilization*

The nature of field appropriation in the sensor basically talks about the bio-molecular interplay between reagents and analytes, as it is highly affected by SPR events. Here, it is worth mentioning that just because of SPR, evanescent field strength reached its peak at the point of reflectance minimum and vice-versa. A vigorous integration due to the effective interaction of charges at the interface of metal-dielectric enhances the strength of the electromagnetic field at the sensing layer [22]. The large evanescent field in the sensing medium enhances the sensing capability of the sensor. Fig. 5(a) displays the distribution of fields at the interfaces of different layers. From Fig. 5(a), it is clearly seen that the maximum electric field arouses at the BP- sensing layer interface, which results in a healthy interaction of the evanescent field with the sensing medium. Whereas, the minimum value of field intensity seen at the prism end is due to the void of the SPR effect. Due to the enhanced electric field intensity at the BP layer and sensing layer interface, the calculated penetration depth of the evanescent field reached a maximum value of 140 nm from the interface. Fig. 5(b) shows the variation of the electric field intensity enhancement factor (EFIEF) and subsequent increase in the RI of the sensing medium. It is clear that the EFIEF decreases with an increase in the RI of the sensing medium. Fig. 5(c) and (d) show the 2-D and 3-D SPs field distributions of the y-directed component of p-polarized light, respectively. The SPP mode is generated by the Cu layer and transitions from Cu to the sensing medium. This clearly shows the symmetrical coupling of SPPs on the interface of the Cu layer, which induces SPPs. Similarly, Figs. 5 (e) and (f) show the 2-D and 3-D field distributions of the y-directed component of the p-polarized light, respectively, for the same optimized SPR sensor design used for the 1-D field plot analysis. Plots show the stronger field distribution at both interfaces of the Cu layer for the SPR sensor design.

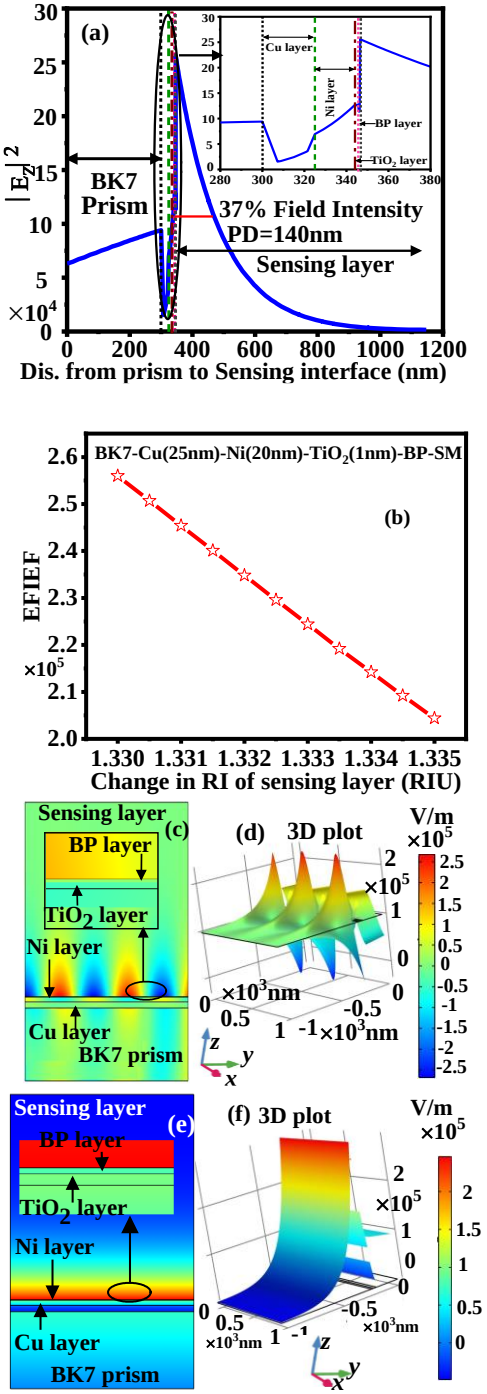

Fig. 5(a) 1D plot of electric field intensity enhancement factor (b) Electric field Intensity enhancement factor (c) 2-D, and (d) 3-D SPP mode (e)2-D, and (f) 3-D electric field distribution at maximum sensitivity.

D. SARS-CoV-2 Detection using Proposed Sensor

In this section, we conduct an analysis of parametric variations by altering the thickness of various layers and the refractive index (RI) of the sensing medium, specifically focusing on the detection of the SARS-CoV-2 virus. We have computed the sensitivity for two distinct RI values associated with SARS-CoV-2, which are 1.3348 and 1.3398. It is important to highlight that both of these RI values are within the predefined RI range of 1.330 to 1.335.

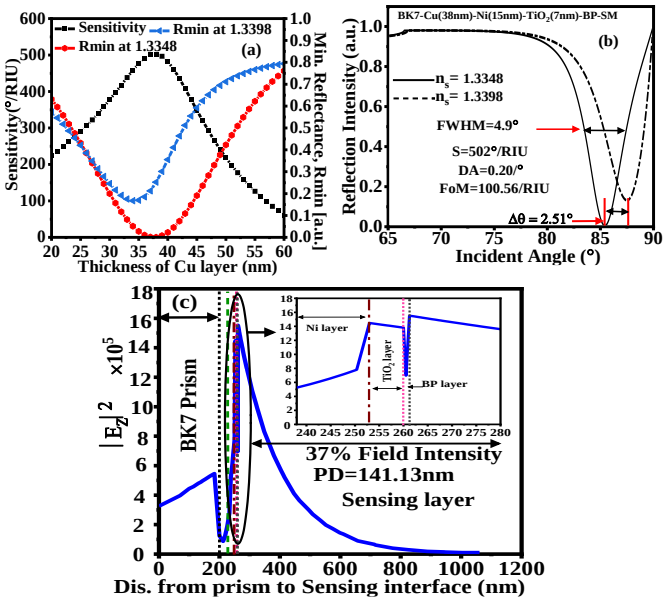

Fig. 6(a) reflectance v/s incident angle (b) sensitivity response with Cu layer thickness, and (c) 1D plot of electric field distribution against the RI variation of SARS-CoV-2.

Fig. 6(a) displays a graph representing sensitivity and the minimum reflectance of the reflectivity plot for two distinct RI values,1.3348 and 1.3398, in relation to changes in the thickness of the Cu layer. Notably, the graph reveals that the minimum reflectance occurs at 38 nm of copper thickness for both RI values, and it's worth highlighting that the highest sensitivity is also achieved at this specific Cu thickness. Interestingly, the sensitivity exhibits an initial increase followed by a decrease as the copper thickness varies. Conversely, the minimum reflectance of the reflectance intensity curve undergoes an initial decrease followed by an increase with varying Cu layer thickness values. In Fig. 6(b), the reflectivity graph for the proposed structure is displayed, showcasing the optimized thickness of each layer. The solid curve corresponds to a sensing layer with RI of 1.3348, while the dotted curve illustrates the graph for a sensing layer with RI of 1.3398. Examining the figure, it becomes evident that the change in the reflectance angle ($\Delta\theta$) amounts to 2.51° for a variation in the RI of the sensing medium of 0.0050. Consequently, the sensitivity of the proposed sensor is calculated to be 502 (°/RIU). In addition, the calculated value of the FWHM is 4.9°, resulting in a detection accuracy of 0.20/°. The FoM is notably high, with a value of 100.56 (1/RIU). The normalized electric field is an important parameter that characterizes the penetration depth (PD) of the proposed sensor. In this proposed sensor, an evanescent electromagnetic field is generated, which is generated by the interaction of light with the Cu surface. The proposed sensor detects the biomolecules. The strength of the evanescent field is proportional to the amplitude of the electric field at the BP surface, and decreases exponentially with distance from the BP surface. The electric field normalized depends on the factor 1/e (approximately 37%). The electric field strength required to achieve SPR under particular conditions is typically chosen as a RI of 1.3348 for the sensing medium. The normalized electric field is then expressed as the ratio of the electric field strength at the BP surface to the sensing medium. The maximum field and PD of 1.5525×10^5 and 141.13 nm are obtained by the proposed sensor,

as shown in Fig. 6(c) at 1.3348 SM. These findings, as observed in Fig. 6, emphasize the sensor's remarkable attributes of high sensitivity and accuracy in detecting the SARS-CoV-2 virus.

IV. Feasibility And Sensor Chip Fabrication With Eroor Possibilities

The essential steps involved in the fabrication of the proposed SPR sensor chip are shown in Fig. 7. First, the BK-7 prism needs to be cleaned by the piranha solution (H_2SO_4:H_2O_2 3:1) at 90°C to remove the organic contaminants [13]. Thereafter, the Cu layer is deposited over the prism by the physical vapor deposition (PVD) technique. Then, the Ni layer is deposited over the Cu layer using PVD and the sputtering technique. After the previous process, the TiO_2 layer is deposited by the same process as the Cu and Ni layers. The BP layer is deposited by

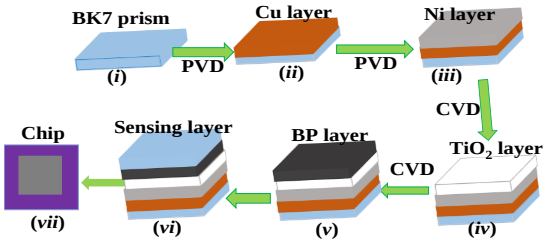

Fig.7 Fabrication process of proposed sensor

the chemical vapor deposition (CVD) technique and can be chemically transferred over the TiO_2 layer [13], [14]. In this way, the SPR sensor chip is prepared and placed over the rotatory base, as shown in Fig. 1 of the SPR sensor setup for sensing purposes. Fabricating the SPR sensor can encounter varying errors depending on design, materials, and techniques. Managing these issues during fabrication is vital for accurate results. Therefore, in our work, the possible manufacturing errors such as thickness variation in all layers i.e., Cu, Ni, TiO_2 and BP are considered, and their effect on sensing performance is shown in Table III.

TABLE III
SENSOR'S PERDOEMANCE WHEN ERROR POSSIBILITY IN 2% AND 3% DECREASE OR INCREASE IN THICKNESS OF ALL CONSTITUENT LAYERS DURING CHIP FABRICATION

Proposed Sensor Structure	Performance parameter	Error possibility in 2% or 3% decrease in thickness		Error possibility in 2% or 3% increases thickness	
		-2%	-3%	+2%	+3%
	S (°/RIU)	471.23	435.44	333.42	161.78
	Rmin.[a.u.]	0.2216	0.258	0.049	0.0110
	FWHM(°)	5.61	5.29	6.4	6.25
	DA (/°)	0.178	0.189	0.156	0.16
	FoM (/RIU)	83.87	82.29	52.01	25.88

TABLE IV
PERFORMANCE COMPARISON OF SUGGESTED SENSOR WITH PRE-EXISTED SPR SENSORS

Sensor configuration	Wavelength (nm)	Sensitivity (°/RIU)	FoM (/RIU)	DA (/°)	Year/Ref.
BK7/Ag/BaTiO3/ Graphene	633	257.00	45.5	-	2019/[33]
CaF_2/ Zno /Au/BP-MoS_2	633	235	56.211	0.281	2021/[8]
BK7/Au/WSe2/PtSe2/BP	633	200	17.77	-	2022/[17]
BK7/Cr/Ag/BP/GO	632.8	352	76.48	0.23	2022/[22]
BP270/Ag/Si/BP/MXene	633	315.79	46.10	0.837	2022/[25]
BK7/ Zno/ Ag/PtSe2/Graphene	633	155.33	21	0.629	2022/[34]
BK7/Cu/Ni/TiO_2/BP	633	516	83.59	0.162	Proposed Work

Table IV showcases the performance metrics achieved by the proposed structure compared to previously published works. It is observed that the proposed sensor's performance is much better than previously reported sensors in terms of sensitivity, FoM, and DA.

TABLE V
PERFORMANCE COMPARISON OF SUGGESTED SENSOR WITH PRE-EXISTED SPR SENSORS FOR SARS-CoV-2 DETECTION

Sensor configuration	Sensitivity (°/RIU)	FoM (/RIU)	Year/Ref.
BK7/Ag/BiFeO3/Graphene	293.81	-	2023/[26]
CaF_2/TiO_2/Ag/BP/Graphene	390	87.95	2023/[32]
BK7/Cu/Ni/TiO_2/BP	502	100.56	This Work

Table V compares the prior state-of-the-art on SARS-CoV-2 detection. The considered sensing parameters, such as sensitivity and FoM, are far better. Hence, the suggested sensor successfully demonstrates its applicability in SARS-CoV-2 virus detection.

V. CONCLUSION

In this article, an ultra-sensitive plasmonic biosensor with hybrid layers of Cu-Ni-TiO_2-BP is proposed for detecting biomolecules in the RI range of 1.330-1.335. Introducing a monolayer of a 2-D nanomaterial, BP, as a sensing layer to the proposed structure significantly enhances the sensing performance due to strong light matter interaction. The TiO_2 layer sandwiched between Ni and BP layers improves sensitivity through magnetic field enhancement at the sensing layer interface. The thickness of the hybrid layers of Cu-Ni-TiO_2-BP has been optimized to 25 nm, 20 nm, 1 nm and 0.53 nm, respectively. As a result, this optimized sensor structure yields a sensitivity of 516°/RIU, which is much higher than the current state-of-the-art research, with remarkable DA, FWHM and FoM of 0.162/°, 6.15° and 83.59/RIU, respectively. Additionally, as an application of a biosensor, the proposed structure is also utilized for the diagnosis of the SARS-CoV-2 virus as its RI values lie in the considered range. The optimum

computed sensitivity for SARS-CoV-2 is 502°/RIU along with DA, FWHM, and FoM to be 0.20/°, 4.9° and, 100.56/RIU, respectively.

REFERENCES

[1] W. L. Then, M.-I. Aguilar, G. Garnier, "Quantitative detection of weak D antigen variants in blood typing using SPR," *Scientific Report*, vol.7, 1-7, 2017.

[2] S. Choudhary, F. Esposito, L. Sansone, M. Giordano, S. Campopiano and A. Iadicicco, "Lossy Mode Resonance Sensors in Uncoated Optical Fiber,"*IEEE Sensors Journal*, vol. 23, no. 14, pp. 15607-15613, July 2023

[3] V. S. Chaudhary, D. Kumar and Santosh Kumar, "Au-TiO_2 Coated Photonic Crystal Fiber Based SPR Refractometric Sensor for Detection of Cancerous Cells," *IEEE Transactions on NanoBioscience*, vol. 22, no. 3, pp. 562-569, July 2023

[4] A. Srivastava, F. Esposito, S. Campopiano, A. Iadicicco, "Mode Transition Phenomena into an in-fiber Mach-Zehnder interferometer" *Optical Fiber Technology*, vol. 80, 103481, Oct., 2023.

[5] F. Esposito *et al*., "The Impact of Gamma Irradiation on Optical Fibers Identified Using Long Period Gratings,"*Journal of Lightwave Technology*, vol. 41, no. 13, pp. 4389-4396, July 2023.

[6] P. S. Pandey, S. K. Raghuwanshi, A. Shadab, Md. T. I. Ansari, U. K. Tiwari,and Santosh Kumar, "SPR based biosensing chip for COVID-19 diagnosis- A review" *IEEE Sensors journal*, vol. 22, pp.13800-13810, 2022.

[7] P. Suvarnaphaet, S. Pechprasarn, "Graphene-based materials for biosensors: A review," Sensors, vol.17, 2161, 2017.

[8] S. Singh, A. K. Sharma, P. Lohia, and D. K. Dwivedi, "Theoretical analysis of sensitivity enhancement of surface plasmon resonance biosensor with zinc oxide and blue phosphorus/MoS_2 heterostructure," *Optik*, vol. 244, 167618, 2021.

[9] J. Homola, ``Present and future of surface plasmon resonance biosensors," *Analytical & Bioanalytical Chemistry*, vol. 377, pp. 528-539, 2003.

[10] J. M. Nijhum, T. Ahmed, M. A. Hossain, J. Atai, N. H. Hai, "Microchannel-embedded D-Shaped photonic crystal fiber-based highly sensitive plasmonic biosensor," *Applied Sciences*, vol. 12, 4122, 2022.

[11] K. L. Lee, C. W. Lee, W. S. Wang, P. K. Wei, "Sensitive biosensor array using surface plasmon resonance on metallic nanoslits," *Journal of Biomedical Optics*, vol. 12, 044023, 2007.

[12] N. Sharma, "Performances of different metals in optical fibre-based surface plasmon resonance sensor," *Indian Academy of Sciences*,vol. 78, pp.417–427, 2012.

[13] Vikash Kumar, S. K. Raghuwanshi, Santosh Kumar, "Nanomaterial-Based Surface Plasmon Resonance Sensing Chip for Detection of Skin and Breast Cancer", *Plasmonics*, 2023.

[14] Prem Kumar, Rajeev Kumar, M. K. Singh, Bilal Ahmed, "A highly sensitive surface plasmon resonance sensor based on black phosphorus in the visible regime", *Opt. and Quant. Electron.*, vol.55, no.12, 2023.

[15] T. Srivastava, R. Jha, R. Das, "High-performance bimetallic SPR sensor based on periodic-multilayer-waveguides," *IEEE Photonics Technology Lett*., vol. 23, pp.1448–1450, 2011.

[16] S. Uniyal, K. Choudhary, S. Sachdev, and Santosh Kumar, "Recent Advances in K-SPR Sensors for the Detection of Biomolecules and Microorganisms: A Review," *IEEE Sensors Journal*, Vol. 22, Issue 22, pp. 11415 – 11426, 2022.

[17] M. Rahman, L. F. Abdulrazak, M. Ahsan, M. A. Based, M. M. Rana, M. S. Anower, K. A. Rikta, J. Haider, S. Gurusamy, "2D nanomaterial-based hybrid structured (Au-WSe2-PtSe 2-BP) surface plasmon resonance (SPR) sensor with improved performance," *IEEE Access*, vol. 10, pp.689–698, 2021.

[18] M. Alagdar, B. Yousif, N. F. Areed, M. Elzalabani, "Improved the quality factor and sensitivity of a surface plasmon resonance sensor with transition metal dichalcogenide 2D nanomaterials," *Journal of Nanoparticle Research*, vol.22, 1–13, 2020.

[19] S. Li, L. Ma, M. Zhou, Y. Li, Y. Xia, X. Fan, C. Cheng, H. Luo, "New opportunities for emerging 2D materials in bioelectronics and biosensors," *Current Opinion in Biomedical Engineering* 13, pp. 32-41, 2020.

[20] M. M. Rahman, M. M. Rana, M. S. Rahman, M. S. Anower, M. A. Mollah, A. K. Paul, "Sensitivity enhancement of SPR biosensors employing heterostructure of $PtSe_2$ and 2D materials," *Optical Materials* 107, 110123, 2020.

[21] R. Kumar, M. K. Singh, L. Garia, B. D. Patel, Mridula, B. M. Singh "Refractive Index Sensing–Based Ultra-Sensitive Black Phosphorus Configured Surface Plasmon Resonance Sensor for the Detection of Glucose Level," *Plasmonics*, 2023.

[22] M. A. Islam, A. K. Paul, B. Hossain, A. K. Sarkar, M. M Rahman, A. S. M. Sayem, R. B. V. B. Simorangkir, M. A. Shobug, J. L. Buckley, K. Chakrabarti, A. Lalbakhsh, "Design and Analysis of GO Coated High Sensitive Tunable SPR Sensor for OATR Spectroscopic Biosensing Applications," *IEEE Access*, vol.10, pp. 103496-103508, 2022.

[23] S. Nangare, P. Patil, "Black phosphorus nanostructure based highly sensitive and selective surface plasmon resonance sensor for biological and chemical sensing: a review," *Critical Review in Analytical Chem.*, vol. 53, no.1, 1–26, 2023.

[24] Y. Singh, M. K. Paswan, S. K. Raghuwanshi, "Sensitivity Enhancement of SPR Sensor with the Black Phosphorus and Graphene with Bi-layer of Gold for Chemical Sensing," *Plasmonics*, vol. 16, pp.1781-1790, Sept. 2021.

[25] Y. Vasimalla, H. S. Pradhan, "Modelling of a novel SCHOTT B270 prism based SPR sensor using Ag-Si-BP/MXene structure for detection of specific biological samples," *Opt. & Quant. Electron.*, vol. 54, 612, August 2022.

[26] S. A. Taya, M. G. Daher, A. H. M. Almawgani, A. T. Hindi, S. H. Zyoud, I. Colak, "Detection of Virus SARS-CoV-2 Using a Surface Plasmon Resonance Device Based on BiFeO3-Graphene Layers," *Plasmonics*, vol. 18, pp.1441–1448, 2023.

[27] I. Astuti, Ysrafil, "Severe acute respiratory syndrome coronavirus 2 (SARS-CoV-2): An overview of viral structure and host response," *Diabetes & Metabolic Synd*rome 14, pp. 407–412, 2020.

[28] M. Gheblawi, K. Wang, A. Viveiros, Q. Nguyen, J-C. Zhong, A. J. Turner, M. K. Raizada, M. B. Grant, G. Y. Oudit, "Angiotensin converting enzyme 2: SARS-CoV-2 receptor and regulator of the renin-angiotensin system," *Circ. Res.* 126, pp.1456–1474, 2020.

[29] J. Wise, "Covid-19: New coronavirus variant is identified in UK," *BMJ* 371, 4857, 2020

[30] F. Cui, H. S. Zhou, "Diagnostic methods and potential portable biosensors for coronavirus disease 2019," *Biosensors & Bioelectronics*, vol. *165, 112349*, 2020.

[31] S. N. Syed Nor, N. S. Rasanang, S. Karman, W. S. W. K. Zaman, S. W. Harun, H. Arof, "A review: Surface plasmon resonance-based biosensor for early screening of SARS-CoV2 infection," *IEEE Access*, vol. 10, pp.1228-1244, 2022.

[32] T. B. A. Akib, S. Mostufa, M. M. Rana, M. B. Hossain, M. R. Islam, "A performance comparison of heterostructure surface plasmon resonance biosensor for the diagnosis of novel coronavirus SARS-CoV-2," *Optical and Quantum Electronics*, vol. 55, 448, 2023.

[33] P. Sun, M.Wang, L. Liu, L. Jiao,W. Du, F. Xia, M. Liu,W. Kong, L. Dong, M. Yun, "Sensitivity enhancement of surface plasmon resonance biosensor based on graphene and barium titanate layers," *Applied Surface Science*, vol.475, 342-347, May 2019.

[34] Moznuzzaman, M., Islam, M.R., Khan, I., "Effect of layer thickness variation on sensitivity: An SPR based sensor for formalin detection," *Sens. Bio-Sensing Res*., vol. 32, 100419, 2021.